Journal of Applied Polymer Science

Morphology and Chain Mobility of Reactive Blend Nanocomposites of PP-EVA/Clay

José M. Mata-Padilla,[1,2] Francisco J. Medellín-Rodríguez,[1] Carlos A. Ávila-Orta,[2] Eduardo Ramírez-Vargas,[2] Gregorio Cadenas-Pliego,[2] Mario Valera-Zaragoza,[3] Sofía M. Vega-Díaz[4]

[1]Centro de Investigación y Estudios de Posgrado, Facultad de Ciencias Químicas, Universidad Autónoma de San Luis Potosí, Av. Dr. Manuel Nava 6, Zona Universitaria, San Luis Potosí, San Luis Potosí, 78210, México
[2]Centro de Investigación en Química Aplicada (CIQA), Blvd. Enrique Reyna Hermosillo 140, San José de los Cerritos, Saltillo, Coahuila, 25294, México
[3]Universidad del Papaloapan, Circuito Central 200, Parque Industrial, Tuxtepec, Oaxaca, 68301, México
[4]Research Center for Exotic Nanocarbons (JST), Shinshu University, Wakasato 4-17-1, Nagano, Japan
Correspondence to: F. J. Medellín-Rodríguez (E-mail: francmr@uaslp.mx or jose.mata@ciqa.edu.mx)

ABSTRACT: Polypropylene (PP)-ethylene vinyl acetate (EVA)/clay nanocomposites were prepared via reactive blending using dicumyl peroxide (DCP) as an initiator with the goal of enhancing the interaction between both phases and modified nanoclay. The effect of the reactive blending and clay incorporation strategies (direct and masterbatch) on the blend and nanostructure morphology, and chain mobility of nanocomposites were studied. The chemical analysis showed the chemical bonding of PP-EVA, which helped to enhance the interaction in the nanocomposites. The nanocomposites obtained from the direct clay strategy presented a co-continuous morphology of bordering intercalated and agglomerated nanoclay sheets, while the nanocomposites obtained from the masterbatch strategy showed that blend morphology change from droplet to co-continuous with the increase of EVA concentration, with intercalated/exfoliated nanoclay sheets located in the EVA domains and at the interface. The dynamic mechanical and creep-recovery results showed different behavior for the both strategies in terms of chain mobility and relaxation. © 2014 Wiley Periodicals, Inc. J. Appl. Polym. Sci. **2014**, *131*, 40897.

KEYWORDS: polyolefins; elastomers; crosslinking; clay; nanostructured polymers

Received 14 January 2014; accepted 17 April 2014
DOI: 10.1002/app.40897

INTRODUCTION

Polymer-clay nanocomposites are a new class of materials which have attracted attention for novel applications in different industrial sectors such as automotive. This interest has increased because these materials often show better mechanical, thermal, physical and chemical properties than the pure polymers.[1,2] However, the improvement in these properties largely depends on the dispersion and exfoliation of the individual nanoclay layers in the polymer matrices, improving the interaction between the clay platelets and polymer chains.[2,3] The exfoliation of individual clay nanosheets can be easily achieved for polar polymers such as polyamides;[4,5] however, in the case of non-polar polymers such as polypropylene (PP), the interactions between the polymer and the polar nanoclay sheets is difficult, decreasing their possible intercalation-exfoliation.[6] An alternative has been to blend polypropylene with a polar polymer, such as poly(ethylene vinyl acetate) (EVA), and a modified clay to obtain an intercalated–exfoliated ternary polymeric nanocomposite, because EVA has been satisfactorily used to generate highly exfoliated nanostructures.[7,8] Additionally, ion-exchanged nanoclays can help the process of polymer chains intercalation within the nanoclay galleries. It has been reported that the molecular characteristics of ion-exchanged surfactants (e.g. the number and length of substitute molecules) can help to exfoliate the clay nanolayers in polymer matrices.[9,10] However, the chemical structure of PP and EVA chains is completely different and therefore the miscibility and compatibility of both macromolecular chains is difficult. It has been reported that the PP/EVA blends are immiscible because they exhibit two or more phases on entire composition and temperatures range.[11–14] Nevertheless, the interfacial adhesion between these immiscible polymers has been enhanced by using different types of compatibilizers. Blend compatibilizers such as maleated Polypropylene (PP-*g*-MA)[14,15] or acrylate Polypropylene (PP-*g*-AA)[16] has been

used to improve the blend compatibility of PP/EVA blends and between PP/EVA and organoclay. Goodarzi et al.,[14] for example, study the effect of different concentration of PP-g-MA compatibilizer on the nanostructure (i.e. intercalated/exfoliated) of PP/EVA blends nanocomposites with different contents of organoclay (OMMT). They reported that blend-based nanocomposites mainly presented intercalated/partially exfoliated structures placed at the EVA phase of the nanocomposites, even at the highest concentration of compatibilizer. In addition, these authors reported that OMMT acted as a compatibilizer reducing the average size of the EVA dispersed phase by preventing coalescence. There are also reports about the action of the OMMTs as compatibilizer of immiscible PP/EVA blends[13] and in different immiscible polymer blend systems such as polystyrene (PS)/polypropylene (PP),[17,18] polypropylene (PP)/ethylene propylene diene monomer rubber (EPDM),[19] and polystyrene (PS)/polymethyl methacrylate (PMMA), polycarbonate (PC)/poly(styrene-*co*-acrylonitrile) (SAN), and polymethyl methacrylate (PMMA)/polyethylene vinyl acetate (EVA).[20] On the other hand, in previous studies on polypropylene (PP)/ethylene vinyl acetate (EVA) and heterophasic polypropylene–(ethylene-propylene) copolymer (PP-EP)/EVA blends, our research group found that there is a compatibility zone at certain composition of PP/EVA and PP-EP/EVA blends. The existence of a disperse EVA phase, in the form of spherical or elongated domains, within a continuous PP and PP-EP phase was observed, correlating the compatibility between the two phases with the size and form of the EVA domains.[12,21] It was also proposed, that the domains size and form depends on the amount of interfacial interactions between the two polymers, affecting the glass transition temperature of both polymers.[22] The morphology of these EVA domains was similar to the morphology of PP-EP/EVA blends, where an organoclay was incorporated.[23–27] However, despite strong interactions between the PP/PP-*g*-MA or PP-EP polymers with EVA, the PP/PP-*g*-MA/EVA/clay and PP-EP/EVA/clay composites have mainly shown intercalated structures, because the compatibility between thermoplastic and elastomeric phase is not high enough to increase the interaction of both phases with nanoclay sheets.[14–16,23–27]

The dynamic crosslinking of elastomer phase in polypropylene blends using DCP as reaction initiator has been also used to increase the compatibility of PP and elastomer polymers such as EVA[11] or EPDM[28] polymers. The increase of compatibility between elastomer (EVA or EPDM) and thermoplastic (PP) phases has been related with the broadening in damping signals of both phases. Additionally, it has been demonstrated that the morphology and dynamic mechanical properties of PP/EVA and PP/EPDM blends was influenced by the reactive blending and blend ratio of thermoplastic and elastomer phases. Particularly, Thomas and George[11] observed that the two phase blend morphology of PP/EVA changed with the blend ratio from droplet morphology at 80/20 ratio to an interpenetrated network (co-continuous) morphology at a 50/50 ratio. Conversely, Katbab et al.[28] reported a two-phase morphology at all PP/EPDM ratios for the dynamically cured samples in which rubber (EPDM) particles are dispersed in the thermoplastic (PP) matrix.

Additionally, the incorporation of clay into polymer matrices modifies the mobility of macromolecular chains due to the interfacial interaction between polymer chains and nanoparticle surfaces. This phenomenon has a significant effect on the rheological (MFI) and dynamical mechanical properties of PP/clay and EVA/clay nanocomposites.[29,30] Comparable behaviors has been reported for ternary systems of PP/PP-g-MA/EVA/clay and PP-EP/EVA/clay nanocomposites.[14,27] Recent work, also show the effect on the stress relaxation behavior of organically modified montmorillonite filled natural rubber/nitrile rubber nanocomposites.[31]

Thus, we proposed that the reactive blending of PP and EVA, using DCP as the initiator, could produce composites with a high degree of clay nanostructure exfoliation within the polymer matrix due to strong interactions between the PP-EVA chains and nanoclay sheets. Moreover, the reactive blending modified the blend morphology and the mobility and relaxation of PP and EVA chains. Therefore, the main aim of this study was to determine the effect of the PP-EVA reactive blending reaction on the interaction between PP-EVA and nanoclay sheets. Additionally, the effects of PP-EVA reactive blending and the clay incorporation strategy on the blend morphology, nanostructure morphology and chain mobility of PP-EVA/clay nanocomposites were studied. For this purpose, direct clay incorporation and masterbatch clay incorporation were tried. The chain mobility of PP-EVA/clay nanocomposites was analyzed using dynamic mechanical analysis and creep-recovery behavior.

EXPERIMENTAL

Materials

PP (MFI 38) of Indelpro, Mexico; EVA (ELVAX 250, MFI25) with 28 wt % of VA from DuPont Co., USA; organoclays (I30E) of Nanocor, Inc., modified with octadecylamine; and dicumyl peroxide, DCP, (98% purity) of FATTA Mexicana were used. The following sections describe the preparation strategies for PP-EVA and PP-EVA/clay nanocomposite samples.

Preparation of PP-EVA/Clay Nanocomposites. Two incorporation strategies for the preparation of PP-EVA/clay reactive blend nanocomposites were used. These are referred as direct and masterbatch strategies and will be described separately in the following sections. A co-rotating, twin-screw extruder (Thyssen) with five heating zones (T1, T2, T3, T4, and T5) was used. The extrusion conditions were a feed rate of 60 rpm and an extrusion rate of 100 rpm.

Direct strategy. The PP-EVA reactive blend (PPEVAx) with a PP:EVA weight ratio of 50:50 and 0.5 wt % of initiator DCP was previously prepared in a twin-screw extruder (see Table I). Then, this sample was used to directly blend two weight concentrations (2 and 6% by weight) of commercial nanoclay (PPEVA2D and PPEVA6D samples, respectively) in a twin-screw extruder. The heating zones profile was T1 = 165°C, T2 = T3 = 170°C, T4 = T5 = 160°C for the PPEVAx sample and T1 = 165°C, T2 = T3 = T4 = T5 = 170°C for both PP-EVA/clay nanocomposites.

Masterbatch strategy. First, a single masterbatch of EVA with 10% by weight of organoclay (MB10C) was prepared using a twin-screw extruder. Subsequently, proportional parts of this

Table I. Summary of Samples Formulation

Sample	PP (wt %)	EVA (wt %)	DCP (wt %)	Clay (wt %)
PPVAx	49.75	49.75	0.5	-
PPEVA2D	48.75	48.75	0.5	2
PPEVA6D	46.75	46.75	0.5	6
MB10C	-	90	-	10
PPEVA2MB	79.75	17.75	0.5	2
PPEVA4MB	59.75	35.75	0.5	4
PPEVA6MB	39.75	53.75	0.5	6

masterbatch were taken and diluted in PP at different PP : EVA weight ratio (80 : 20, 60 : 40, and 40 : 60, respectively) to obtain nanocomposites with 2, 4, and 6 wt % of clay. Then, 0.5 wt % of DCP was added to each sample, and finally, all components were reactively blended in a twin-screw extruder under the same extrusion conditions as the direct strategy samples. Table I contains descriptions of the formulations used to prepare the PPEVAx and respective nanocomposite samples (PPEVA2MB, PPEVA4MB, and PPEVA6MB).

PP-EVA Extractions

The methodology used to extract unreacted polymers from the PPEVAx sample was performed in two parts: In the first part, the PPEVAx sample (18 g) was put into a jar containing 150 mL of toluene and was left without agitation for 7 days at room temperature. The solid was separated (S1), and the solution was concentrated in a rotary evaporator under vacuum and then precipitated in methanol. The precipitated polymer (E1) and the solid (S1) were dried in a vacuum oven (70°C, 5 hours). Then, the solid (S1) was again put into a jar containing toluene and left without agitation for 4.5 days at 40°C. The solid (S1′) was separated, and the solution (E1′) was concentrated in a rotary evaporator and precipitated in methanol. The extracted polymer (E1′) and the solid (S1′ = 14.3g) were dried in a vacuum oven. The extracted polymer samples (E1 and E1′ = 3.7 g) were combined for analysis. The second part was realized using a soxhlet extraction device. The solid S1′ (14.3 g) was put into a soxhlet extraction device using THF as the solvent. The extraction was performed over 30 h, obtaining a third extracted polymer (E2 = 0.9 g) and solid (S2 = 13.4g), which were dried in a vacuum oven. Later, the solid S2 was again placed into the soxhlet device with toluene for 30 h, obtaining the precipitated polymer (E3 = 0.35g) and the residual solid (S3 = 13.05g), which were dried under the same conditions as the first samples. Finally, the solid S3 was separated into two parts, R1 (translucent solid) and R2 (opaque solid).

Characterization

Crosslinking Degree. The degree of crosslinking of PPEVAx and PP-EVA/clay nanocomposite samples obtained through masterbatch strategy was determined according to ASTM-D2765. A 120 mesh wire cage with 0.500 g ± 0.020 (Ws) of every sample was placed into a 200 mL jar with 100 mL ± 0.1 mL of xylene, and they were boiled for 12 h. Afterwards, the wire cages were removed and placed in a vacuum oven at 100°C until the xylene was completely removed. Finally, the samples were weighed again (Wd). The crosslinking degree was determined as a function of the gel content (%) presented in each sample:

$$\text{Gel}\,\% = \left(1 - \frac{W_s - W_d}{W_0}\right) \times 100\% \quad (1)$$

where W_s = weight of specimen being tested, W_d = weight of dried gel, and W_o = original polymer weight.

Melt Flow Index. The melt flow index (MFI) of raw polymers (PP, EVA), PPEVAx, and all PP-EVA/clay nanocomposites was determined according to ASTM-D1238 using a Melt Flow Indexer LMI 300 from Dynisco (USA). A brief protocol used in MFI determination according to ASTM-D1238 is described: It was firstly selected the conditions of temperature (230°C) and load (2.16 kg) accordance with material specifications. Then, it was charged the cylinder within 1 min with a weighed portion of the sample (4.0–8.0 g) in accordance with the expected flow rate and then purges some melted material. Finally, for all tests, the timed extrudate was collected to the required piston position.

Fourier-Transformed Infrared (FT-IR) Spectroscopy. The FTIR analysis of PPEVAx, MB10C, and PP-EVA/clay nanocomposite samples obtained by the masterbatch strategy was performed in a Nicolet spectrometer using Attenuated Total Reflectance (ATR) of Pike, with a germanium crystal, at a resolution of 4.0 cm^{-1} over a wave number range of 400 to 4000 cm^{-1}.

Differential Scanning Calorimetry (DSC). Thermal experiments of the PPEVAx sample extractions (E1 and E2) and residues (R1 and R2) were performed in a differential scanning calorimeter DSC-2029 from TA instrument. This calorimeter was calibrated with an indium standard under a constant nitrogen flow in both the sample and reference chambers. All samples weighted 8 ± 1 mg and were sealed within aluminum pans before positioning them in the sample holder. Samples were heated from room temperature at 10°C/min up to 190°C.

Small-Angle X-ray Scattering (SAXS). The nanostructure analysis was developed using the SAXS technique. This study was performed in a SAXSess mc2 system from Anton Paar, using Imaging Plates as the X-ray detector. SAXS 2D patterns were obtained at exposure times of 10 min. Each 2D pattern was integrated from 0° to 180° to obtain 1D SAXS patterns.

Scanning Electron Microscopy (SEM). To study the blend morphology of different PP-EVA/clay nanocomposites, the surface of cryogenically fractured injection-molded samples was etched with toluene at 40°C for 2 h to remove the EVA phase and then observed using a JSM-7401F Field Emission Scanning Electron Microscope (FESEM) from JEOL. Before imaging, samples were sputter-coated with a mixture of Au-Pd. The SEM micrographs were taken at an accelerating voltage of 6 kV.

Transmission Electron Microscopy (TEM). This technique was used to observe the nanoparticle dispersion within the polymer matrix and the nanocomposite structure. Pieces of EVA/clay masterbatch and different PP-EVA/clay nanocomposites with dimensions of 1 cm × 1.5 cm × 0.08 cm were prepared. Each

sample was cut cryogenically to an approximate thickness of 90 nm with a microtome. Both a JEOL TEM 1200EX with a Lanthanum Hexaboride glass as an electron source and a FEI TEM Titan 80–300 were used. The operating voltages used were 100 keV (JEOL TEM 1200EX) and 300 keV (FEI TEM Titan 80–300).

Dynamic Mechanical Analysis (DMA). Dynamic mechanical properties for PPEVAx and the different PP-EVA/clay nanocomposites, obtained using the two different clay incorporation strategies, were determined. To perform this analysis, rectangular sections of molded parts (3 cm × 1.2 cm × 0.3 cm) were used. The analysis was performed at a heating rate of 3°C/min from −80°C to 80°C, at amplitude of 3°C and a frequency of 1 Hz in a dynamic mechanical analyzer DuPont TA-983.

Creep and creep-recovery test. Creep and creep–recovery tests were conducted in tensile mode at 30°C using a dynamic mechanical analyzer (DuPont TA-983). The size of the specimens for creep and recovery tests was 25 mm x 5 mm x 0.7 mm. The creep and recoverable strain were determined as functions of the time ($t_{creep} = 30$ min and $t_{recovery} = 60$ min). The stress level was fixed at 1 MPa to ensure that the creep measurements remained in the linear viscoelastic deformation regime.

Theoretical background. During a typical creep test, the stress, σ is applied at $t = 0$ and is kept constant until $t = t_0$, when the stress is removed. In the general case, the strain response (ε) consists of three components:

$$\varepsilon(t,\sigma) = \varepsilon_e(\sigma) + \varepsilon_{ve}(t,\sigma) + \varepsilon_{vp}(t,\sigma) \quad (2)$$

where indexes e, ve, and vp correspond to the elastic, viscoelastic and viscoplastic strain components, respectively. Usually, polymer composites exhibit a nonlinear viscoelastic response, which appears in a stress-dependence of the creep compliance $J(t)$. This response is defined as:

$$J(t) = \varepsilon(t)/\sigma \quad (3)$$

where $\varepsilon(t)$ = strain at $t = t$ and σ = applied stress.

On the other hand, viscoplastic effects are observed as irreversible strains remaining for a certain amount of time after the stress is removed. The recovery time should normally be at least three times longer than the creep time. Equation (2) is possible only by assuming that the viscoelastic and viscoplastic responses are decoupled.

RESULTS AND DISCUSSION

Chemical Aspects of PP-EVA Reactive Blends

During the reactive blending of PP and EVA using DCP as the initiator, the crosslinking of the EVA phase and/or the degradation of the PP phase by β-scission have been reported.[11] These reactions have been highly influenced by several parameters, such as the blend composition and viscosity ratio.[11,32–35] Therefore, the blend composition and viscosity ratio used in this study for PP-EVA reactive blending were almost 1 : 1 to decrease these reactions. In this work, the reactive blending of PP and EVA using DCP as the initiator produced different products to be analyzed. Therefore, solvent extractions with toluene and THF were performed, obtaining two different

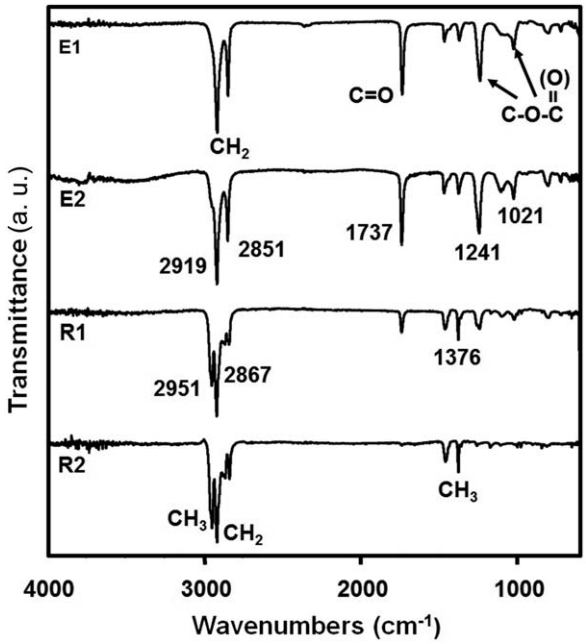

Figure 1. FT-IR spectra for extracted samples (E1 and E2) and residues samples (R1 and R2) of PPEVAx sample after the toluene and THF extractions.

extractions (E1 and E2) and two residue products (R1 and R2). The FTIR spectra of the extractions and residues are presented in Figure 1. The FT-IR spectra of the E1 and E2 samples show a characteristic EVA infrared spectrum, which is related to carbonyl group (C = O) (1737 cm^{-1}), C-O group associated with the vinylacetate (VA) unit (1241 and 1021 cm^{-1}) and CH_2 group associated to ethylene unit (2919 and 2851 cm^{-1}). Additionally, the R1 sample presented an infrared spectrum with characteristic bands of polypropylene (2951, 2867, and 1376 cm^{-1}) and EVA (2919, 2851, 1737, 1241 and 1021 cm^{-1}), while the R2 sample mainly presented a polypropylene IR spectrum. This behavior indicates that the PPEVAx sample was mainly composed of a PP-EVA copolymer, with some uncrosslinked and crosslinked EVA and polypropylene. Therefore, the PP and EVA ratio used in this work significantly decreased the EVA crosslinking and PP β-scission reactions and enhanced the bonding between the PP and EVA chains.[11,34] This behavior has also been observed before for grafting copolymerization of PP with unsaturated functional monomers such as maleic anhydride using DCP as the initiator.[36,37]

The heating thermograms of DSC for residues and extractions are shown in Figure 2. Here, it is observed that both extractions (E1 and E2) present endothermic two peaks related to polyethylene section of EVA ($T_m \approx 50$ and 66°C).[38] However, the R1 sample presents two endothermic peaks at approximately 50 and 65.5°C, related to the melting of EVA phase, and an endothermic peak at 164.3°C, corresponding to the melting of PP phase. This thermal behavior indicates the immiscibility of the polymers, while their compatibility, in the amorphous region,[39] remained due to the reactive blending of PP and EVA polymers. Finally, the R2 sample presented a DSC melting trace of polypropylene with a melting peak at 165.5°C. Last thermal

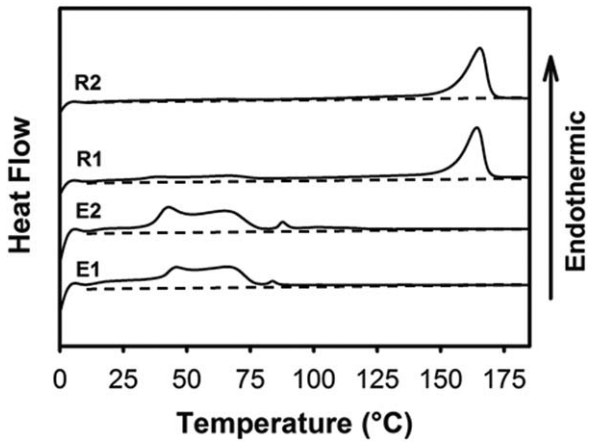

Figure 2. DSC heating traces of extractions samples (E1 and E2) and residues samples (R1 and R2) of PPEVAx sample after the toluene and THF extraction.

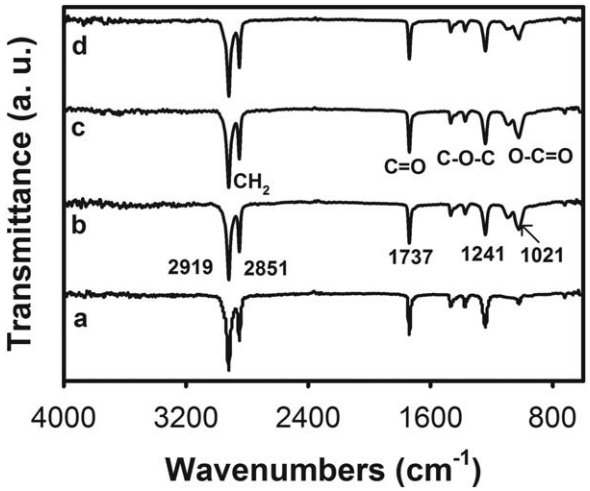

Figure 3. FT-IR spectra of gel residues for: a) PPEVAx, b)PPEVA2MB, c) PPEVA4MB and d) PPEVA6MB samples.

behavior corroborated the results observed by the FT-IR spectra for different extractions (E1 and E2) and residues (R1 and R2).

However, it was necessary to determine the possible crosslinking degree of the elastomer phase due to the reactive blending of PP and EVA polymers. This crosslinking degree can be associated with the gel content. The gel content for the PPEVAx sample was 13.42% (see Table II). The results of the gel content showed that the reactive blend PPEVAx produced a low degree of crosslinking. This result is in agreement with different observations from various authors, where a 1 : 1 weight ratio of PP and EVA reduced the EVA crosslinking reaction.[11,34] Conversely, the gel content of PP-EVA/clay nanocomposites prepared through the materbatch strategy increase with the EVA concentration in the blend. The chemical composition of all gels is shown in the ATR-FT-IR spectra (Figure 3). This figure shows a typical FT-IR spectrum of EVA for all samples. According with the results showed in this section, a probable reaction progress of the polypropylene (PP) and ethylene vinyl acetate (EVA) using DCP as initiator is showed in Scheme 1.

Blend Morphology

The reactive blend morphology of PP-EVA/clay nanocomposites prepared through the direct strategy with 2 and 6% of organoclay was analyzed by SEM. Figure 4 presents the SEM micrographs of PPEVA2D and PPEVA6D samples. These figures shows that for PP-EVA/clay nanocomposites prepared through direct strategy, the un-crosslinked EVA formed a co-continuous phase (interpenetrated network, IPN) with a blend of PP-EVA copolymer, crosslinked EVA and PP. This blend morphology has been previously related to some grade of compatibility between PP and EVA phases in dynamical crosslinking PP/EVA blends[11] and in PP/EVA/clay nanocomposites systems using PP-*g*-MA as compatibilizer.[14,15] In the case of this work, the compatibility is attributed to the dynamic crosslinking reaction which increases the interfacial interaction between PP and EVA phases. However, there is not observed a significant effect of the organomodified clay introduction on the compatibility of the PP and EVA phases, in disagreement to that reported for different immiscible polymer blends nanocompounded with nanoclays,[13,14,17–20] where an average size reduction of the dispersed phase was reported. This effect has been attributed to the localization of nanoclay sheets in the interface between the dispersed and continuous phases.

Table II. Gel Percentage (%) for PPEVAx Sample and PP-EVA/Clay Nanocomposites Obtained by Masterbatch Strategy with 2, 4, and 6 wt % of nanoclay After the Extraction with Boiled Xylene

Sample	%Gel
PPEVAx	13.42
PPEVA2MB	11.90
PPEVA4MB	23.95
PPEVA6MB	43.72

Conversely, Figure 5 shows the SEM micrographs of PP-EVA/clay nanocomposites prepared through masterbatch strategy. Figure 5(a) shows that PPEVA2MB presents irregularly joined droplet morphology of the un-crosslinked EVA phase dispersed into the continuous blend of PP, PP-EVA copolymer and crosslinked EVA phase, as it was observed in PP/PP-*g*-MA/EVA/clay based blend nanocomposites[14] and PP-EP/EVA/clay nanocomposites at PP/EVA ratio of 80/20.[24] However, when the proportion of EVA increases to ≈36% (PPEVA4MB sample) and 54% (PPEVA6MB sample), the uncrosslinked EVA tends to form a continuous phase until to be in a co-continuous IPN morphology with the PP and PP-EVA copolymer. The co-continuous nature of these phases is due to the higher proportion of EVA and the low melt viscosity of PP and PP-EVA copolymer.[11]

In this work, the composition and viscosity ratio of the PP-EVA reactive blend generated a blend morphology, which helped to disperse nanoclays and enhanced the interaction of nanoclay sheets with PP and EVA domains. Figure 6 presents the TEM micrographs of PPEVA2D and PPEVA2MB samples at low magnifications. Figure 6(a) shows that the PPEVA2D sample mainly presents a co-continuous morphology bordered by intercalated

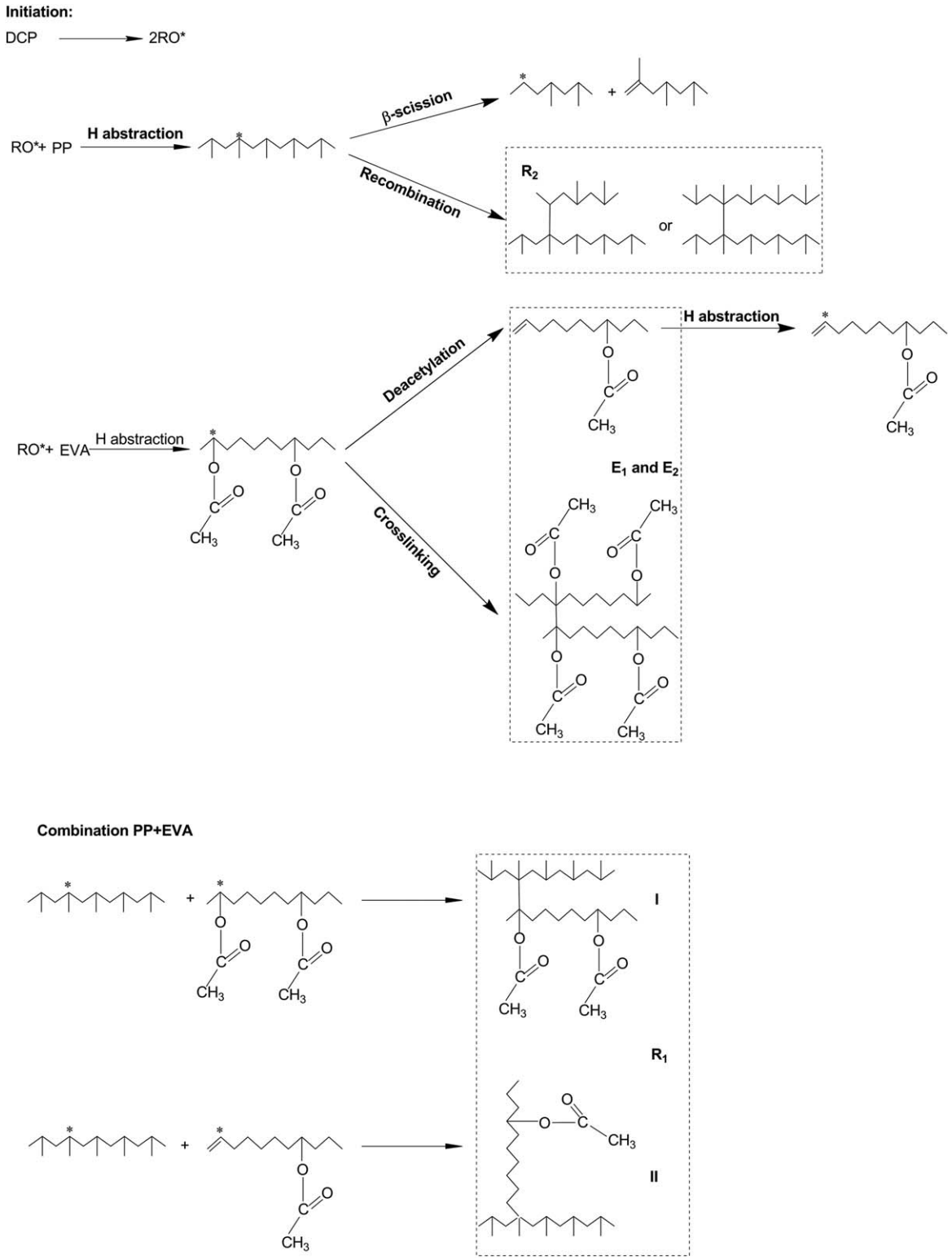

Scheme 1. Possible reaction progress of the polypropylene (PP) and ethylene vinyl acetate (EVA), using DCP as initiator. The possible chemical structure bond of E1, E2, R1, and R2 samples is shown.

and agglomerated nanoclay sheets,[14,38,40] where the irregular domains are conformed by PP-EVA copolymer chains and by uncrosslinked and crosslinked EVA chains. Additionally, Martins et al.[16] reported that the presence of clay platelets at the interface between PP and EVA led to the irregular shape of the EVA particles by hindering the rounding promoted by the interfacial tension in the neat PP/EVA blend. Nevertheless, the nanocomposites obtained using the masterbatch clay introduction

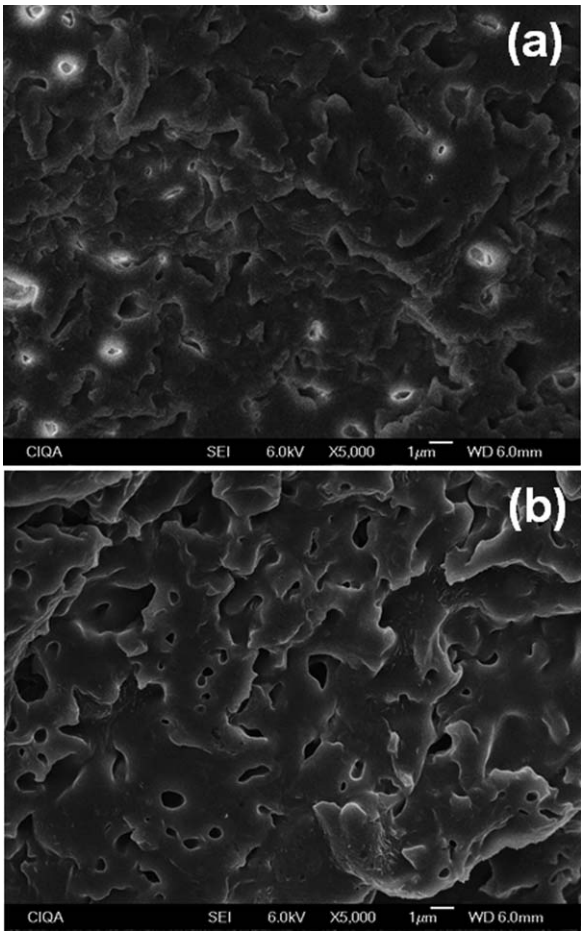

Figure 4. SEM micrographs of PP-EVA/clay nanocomposites prepared through the direct strategy: a) PPEVA2D b) PPEVA6D.

strategy presented different morphologies as a function of the PP/EVA concentration ratio. Figure 6(b) presents the irregularly joined droplet morphology of the EVA phase dispersed into the continuous PP phase for the PPEVA2MB sample, previously observed in Figure 5(a).[26,40–43] The reaction of PP and EVA using DCP and the previous introduction of nanoclay into the EVA matrix (masterbatch) caused the joined anisotropic morphology for this nanocomposite. Figure 6(a′,b′) show a schematic representation of the different blend morphologies for PPEVA2D and PPEVA2MB samples.

Nanostructure Morphology

Direct Incorporation Strategy. Figure 7 shows the SAXS patterns of nanoclay I30E and the PPEVA2D and PPEVA6D samples. For both nanocomposites, the d_{001} peak shifted to lower angles (37.6 Å and 35.4 Å)with respect to the peak of the I30E organoclay (22.7 Å), suggesting the intercalation of PP-EVA molecules into the clay galleries in agreement to values reported in the literature for different nanocomposites of PP-EVA/organoclay and PP-EP/EVA/organoclay.[14,16,23,27] The larger d-spacing for the PPEVA2D nanocomposite (37.6 Å) than for the PPEVA6D nanocomposite (35.3 Å), see Table III, suggested greater intercalation at low clay concentrations. However, the intercalation degree for both nanocomposites was of the same order of magnitude. This result suggested that the incorporation of EVA macromolecules to PP macromolecules through the previous reactive blending, the high d-spacing of I30E nanoclay (22.7 Å) and the nature of the clay modifier (octadecylamine) helped to intercalate some PP chains into the clay galleries.

TEM micrographs of the PPEVA2D and PPEVA6D nanocomposites at different magnifications are presented in Figure 8. Figure 8(a,b) shows an intercalated morphology for the nanoclay I30 E

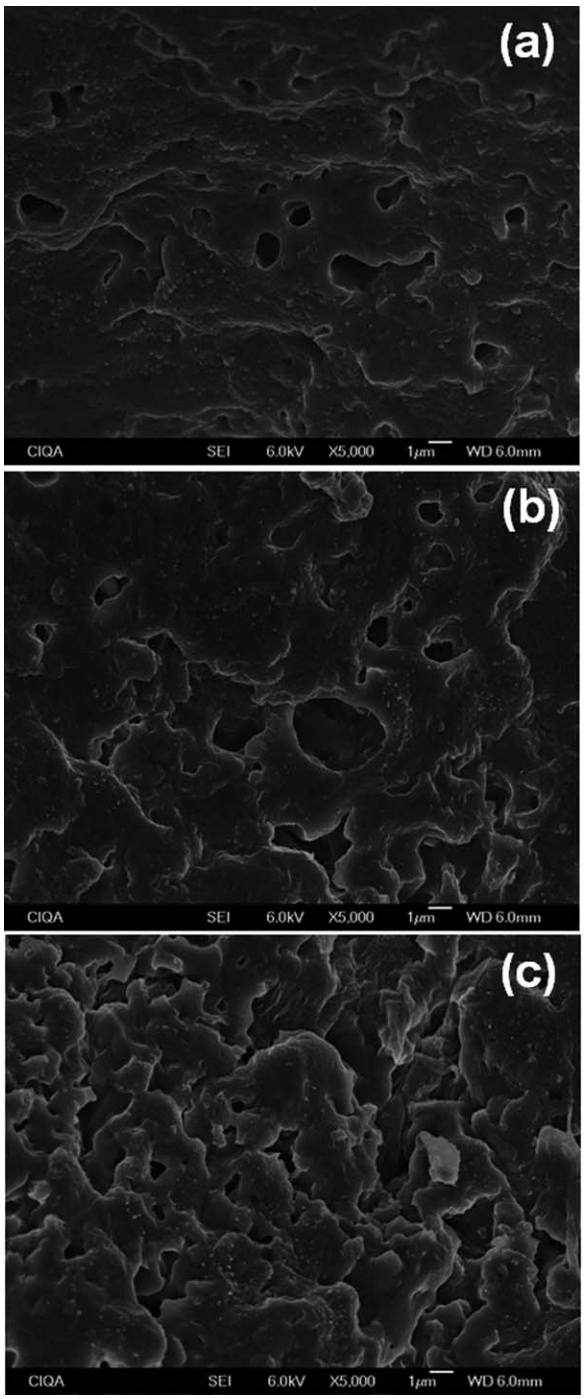

Figure 5. SEM micrographs of PP-EVA/clay nanocomposites prepared through the masterbatch strategy: a) PPEVA2MB, b) PPEVA4MB, c) PPEVA6MB at high magnification.

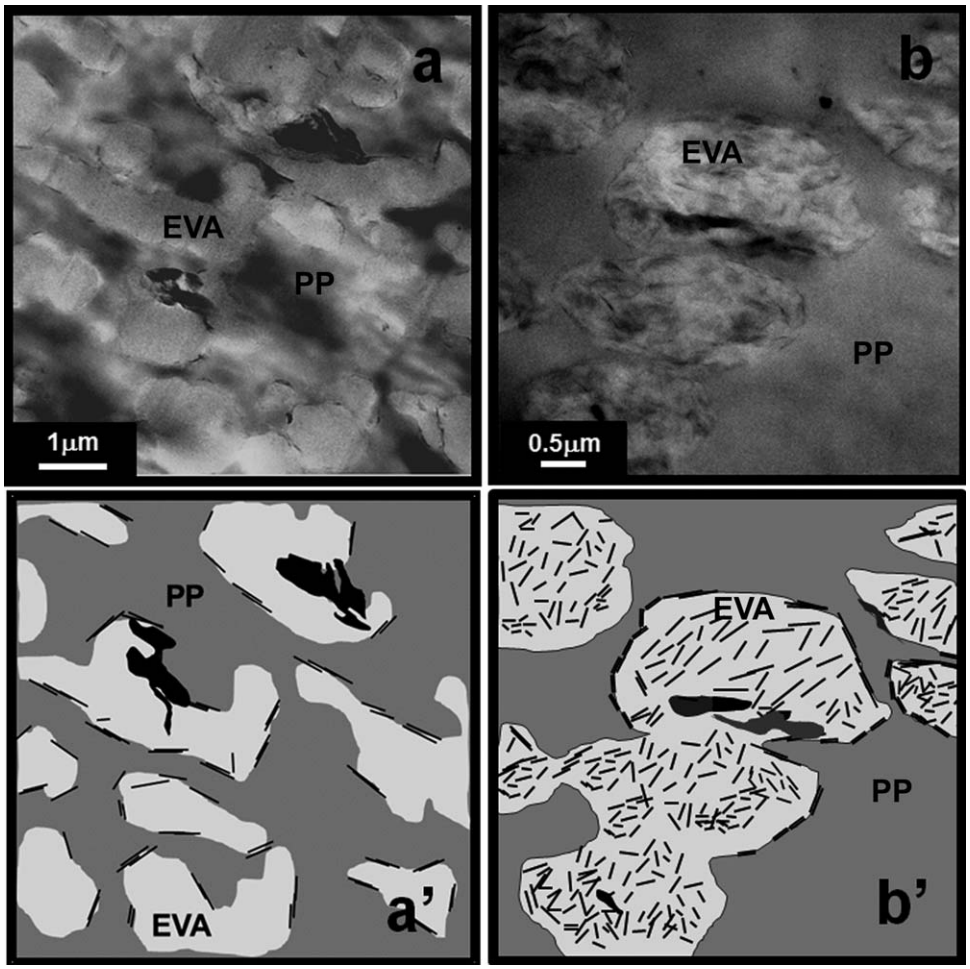

Figure 6. Low magnification TEM micrographs and schematic draw of blend morphology for: a and a′) PPEVA2D and b and b′) PPEVA2MB.

into the PP-EVA matrix for both clay concentrations (2 and 6 wt %) at low magnifications (5×). Some tactoids of nanoclay sheets (see arrows) are also observed. Moreover, higher magnifications TEM micrographs (20×) shown in Figure 8(c,d) corroborate the intercalated morphology observed at lower magnifications. However, the intercalation degree was not highly dependent on nanoclay concentration. This behavior is consistent with the previous SAXS results and with the morphologies reported for different types of PP/EVA/clay nanocomposites.[14,16]

Masterbatch Incorporation Strategy. Figure 9 shows the SAXS patterns of nanoclay I30E, EVA/clay masterbatch and the nanocomposites of PP-EVA with 2%, 4%, and 6% of nanoclay prepared using the masterbatch incorporation strategy. For the EVA/clay masterbatch and all nanocomposites, the d_{001} peak shifts to lower angles with respect to the peak of the I30E organoclay and the nanocomposites prepared by direct incorporation strategy, suggesting a higher intercalation degree of the PP-EVA molecules into the clay galleries. The d-spacing for the EVA/clay masterbatch (38.2 Å) is similar to values reported in the literature for different nanocomposites of EVA/organoclay.[14,16,24,27] However, the d-spacing of PP-EVA nanocomposites with 2, 4, and 6% of clay (46.2, 42.0, and 42.0 Å, respectively) obtained for the masterbatch strategy was higher than the values reported for the PP/EVA/clay nanocomposite,[14–16] and the larger d-spacing for the PPEVA2MB nanocomposite with respect to PPEVA4MB and PPEVA6MB nanocomposites, suggests greater intercalation of PP-EVA molecules into the clay

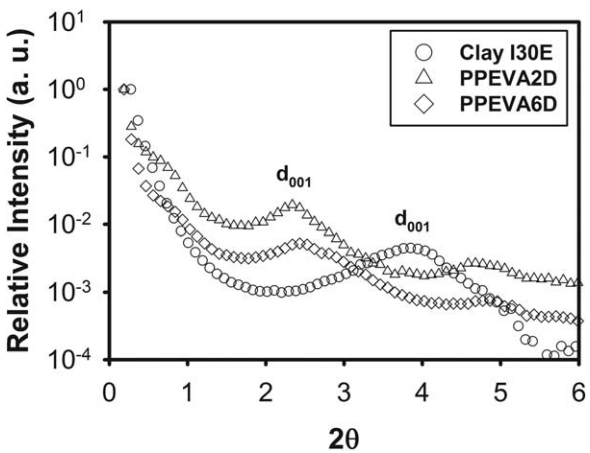

Figure 7. SAXS patterns of nanoclay I30E and PP-EVA/clay nanocomposites obtained through direct strategy.

Table III. *d*-Spacing of Organoclay I30E, MB10C, and PP-EVA/Clay Nanocomposites Obtained by Direct (D) and Masterbatch (MB) Strategies, After Lorentz Correction

Sample	*d* (Å)
CLAY I30E	22.7
PPEVA2D	37.6
PPEVA6D	35.3
MB10C	38.2
PPEVA2MB	46.2
PPEVA4MB	42.0
PPEVA6MB	42.0

galleries at lower clay concentrations. Moreover, the scattering intensity of the MB10C and the three nanocomposites of PP-EVA decreased significantly with respect to the scattering intensity of nanoclay I30E, indicating that the MB10C sample and the PP/EVA/clay nanocomposites prepared via the masterbatch strategy have an intercalated/exfoliated nanostructure, according to the observations of Vaia and Giannellis[44] and Morgan and Gilman.[45] To probe this proposition, the structural nanocomposite morphology was determined using TEM observations.

TEM micrographs of the EVA/clay masterbatch, PPEVA2MB, PPEVA4MB and PPEVA6MB nanocomposites at different magnifications are presented in Figure 10. Low magnification micrographs [Figure 10(a–d)] mainly show intercalated/exfoliated clay morphology in the MB10C sample; however, a high exfoliation degree is observed. Additionally, the nanostructure at low clay concentration (2 wt %) present an intercalated/exfoliated morphology with a high amount of exfoliated clay sheets, while an increase in the nanoclay concentration (i.e., 4 and 6 wt %) leads to the formation of a mixed nanostructure (intercalated/exfoliated) with few tactoids. Espinoza-Martínez et al. reported the presence of two nanoclay populations (intercalated/exfoliated and tactoids) in PP-EP/EVA/clay systems as a function of the VA concentration in EVA polymers,[26] and they also noticed the disappearance of tactoids at the highest VA concentrations in EVA. High magnification TEM micrographs of the EVA/clay masterbatch and all nanocomposites are shown in Figure 10(e–h). These figures corroborate the highly exfoliated and intercalated/exfoliated nanostructures observed at lower magnifications for MB10C, PPEVA2MB, PPEVA4MB, and PPEVA6MB samples.

Chain Mobility and Relaxation

Figure 11(a,b) shows the storage modulus (E') versus temperature results for direct and masterbatch strategy nanocomposites.

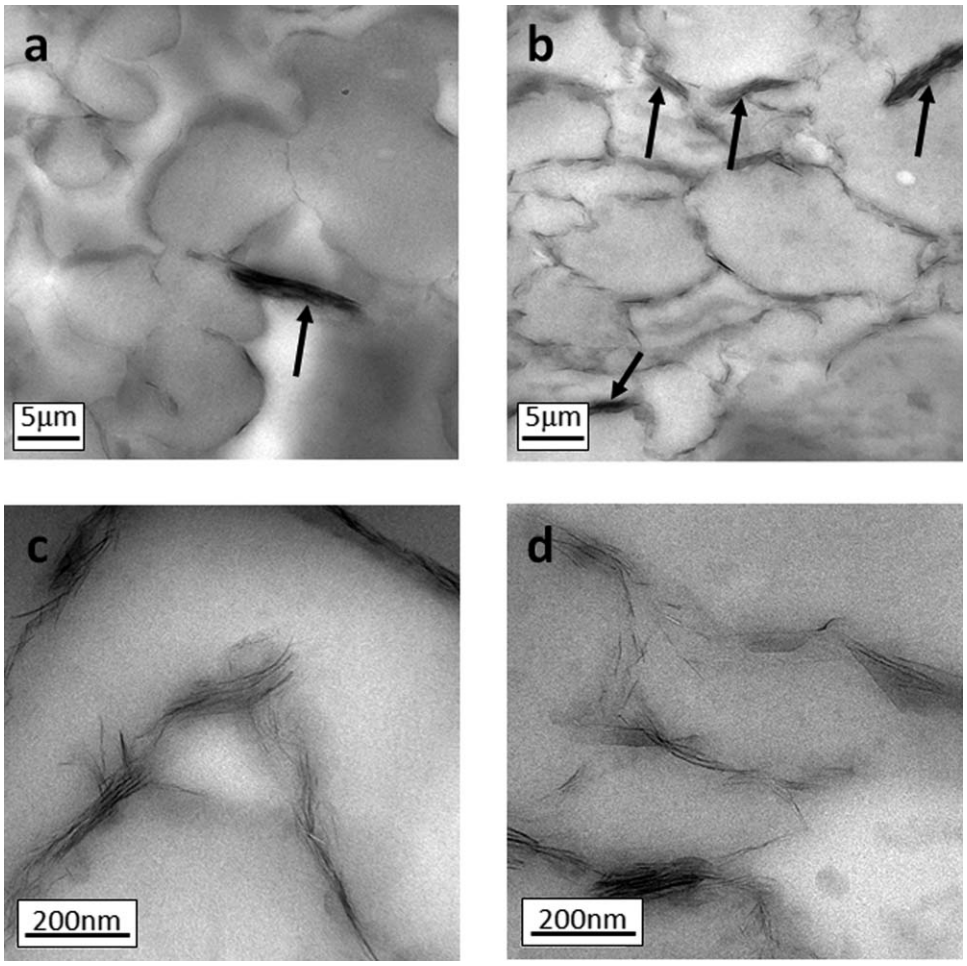

Figure 8. TEM micrographs at low and high magnifications of PP-EVA/clay nanocomposites obtained by direct strategy: a) PPEVA2D (low), b) PPEVA6D (low), c) PPEVA2D (high), and d) PPEVA6D (high). Tactoids are pointed out with arrows.

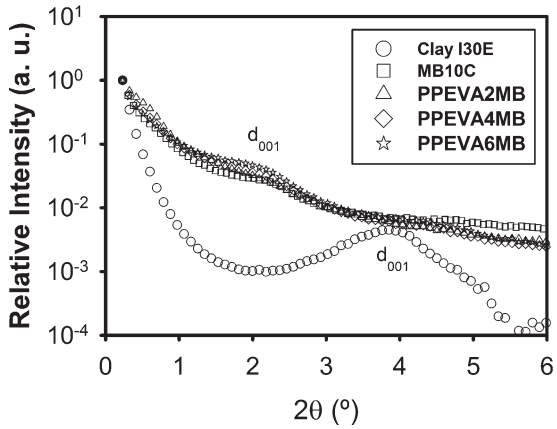

Figure 9. SAXS patterns of nanoclay I30E, EVA/clay masterbatch and PP-EVA/clay nanocomposites obtained through masterbatch strategy.

Figure 11(a) shows that clay introduction within the PPEVAx sample increased the storage modulus at low temperatures (−80°C) from 2050 MPa to 2200 and 2450 MPa for nanocomposites with 2 wt % and 6 wt %, respectively. Goodarzi et al.[14] proposed that the simultaneous incorporation of nanoclay and compatibilizer (PP-*g*-MA) leads to a monotonous increase in *E*' values for PP/EVA/clay samples due to the penetration of both PP and PP-*g*-MA chains into the nanoclay layers and their immobilization inside the silicate galleries. On the other hand, Valera-Zaragoza et al.,[27] reported an increase of E' with the concentration of nanoclay in a PP-EP/EVA system, attributing to the confinement of the polymer chains within the clay interlayer space and by the interactions with the clay nanolayers. In agreement, the increase of storage modulus, in this work, could be attributed to the decrease of chain mobility of PPEVAx macromolecules because their high interfacial interactions with

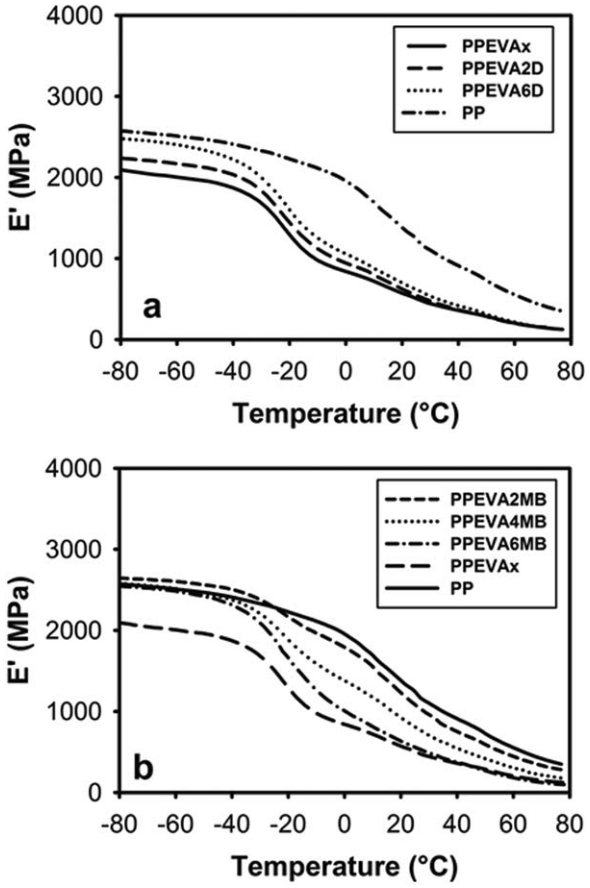

Figure 11. Storage modulus (*E*') versus temperature of: a) PPEVAx and PP-EVA/clay nanocomposites obtained by direct strategy and b) PP homopolymer, PPEVAx and PP-EVA/clay nanocomposites obtained by masterbatch strategy.

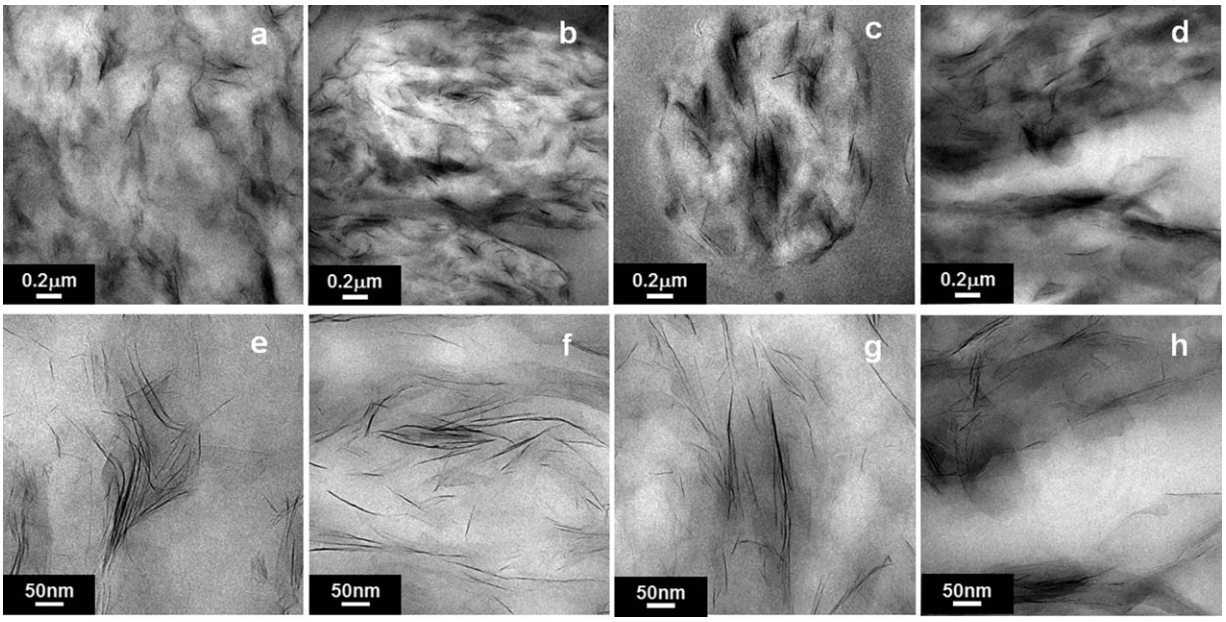

Figure 10. TEM micrographs at low (a–d) and high magnifications (e–h) of PP-EVA/clay nanocomposites obtained by masterbatch strategy: a) and e) MB10C, b) and f) PPEVA2MB, c) and g) PPEVA4MB, d) and h) PPEVA6MB samples.

Table IV. Melt Flow Index (MFI) of PP and EVA Homopolymers, PPEVAx Sample, and PP-EVA/Clay Nanocomposites Obtained by Direct (D) and Masterbatch (MB) Strategies

Sample	MFI[a] (g/10 min)
PP	90.4
EVA	59.5
PPVAx	5.4
PPEVA2D	13.6
PPEVA6D	10.1
PPEVA2MB	81.1
PPEVA4MB	25.4
PPEVA6MB	1.0

[a] ASTM-D1238.

intercalated clay sheets, which act as a non-melting crystalline phase.[46–48] On the other hand, the mechanical behavior of both nanocomposites at temperatures greater than the T_g of both polymers is nearly identical. However, the chain mobility of PP-EVA matrix in the melt state conditions was increased due to the introduction of clay nanoparticles,[29,30] such as the MFI values (Table IV) showed. This table reported that the PPEVAx sample has an MFI = 5.4 g/10 min, while the PPEVA2D and PPEVA6D samples have MFI = 13.6 and 10.1 g/10 min, respectively. Last behavior indicates that the introduction of nanoclay can enhance the processability of PPEVAx during different plastic manufacturing processes such as injection or compression molding.

The E' versus T results presented in Figure 11(b) show that the PPEVA2MB sample presents a higher storage modulus, in brittle and leathery regions, than nanocomposites with 4 and 6 clay % because the amount of EVA phase was lower than in PPEVA4MB and PPEVA6MB samples. The storage modulus decrease has been previously related to increase of elastomer phase in dynamically cured PP/EPDM thermoplastic elastomer.[28] However, the differences in the storage modulus at low temperatures (−80°C) between samples (2645, 2581, and 2545 MPa, respectively) are lower because PPEVA4MB and PPEVA6MB nanocomposites have an intercalated/exfoliated nanostructure, which helps to decrease the chain mobility in the melt state (see MFI index in Table IV), compared to the PPEVA2MB sample (mainly exfoliated structure). Additionally, the storage moduli for all nanocomposites obtained via the masterbatch strategy are higher than the PPEVAx sample over all temperature ranges.

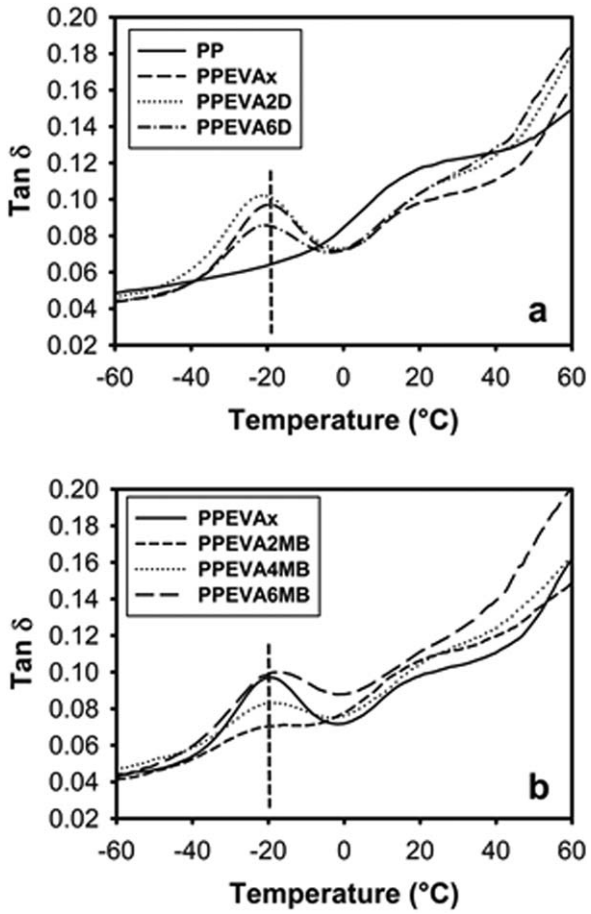

Figure 12. Tan δ versus temperature of: a) PP homopolymer, PPEVAx and PP/clay nanocomposites obtained by direct strategy and b) PPEVAx and PP-EVA/clay nanocomposite obtained by masterbatch strategy.

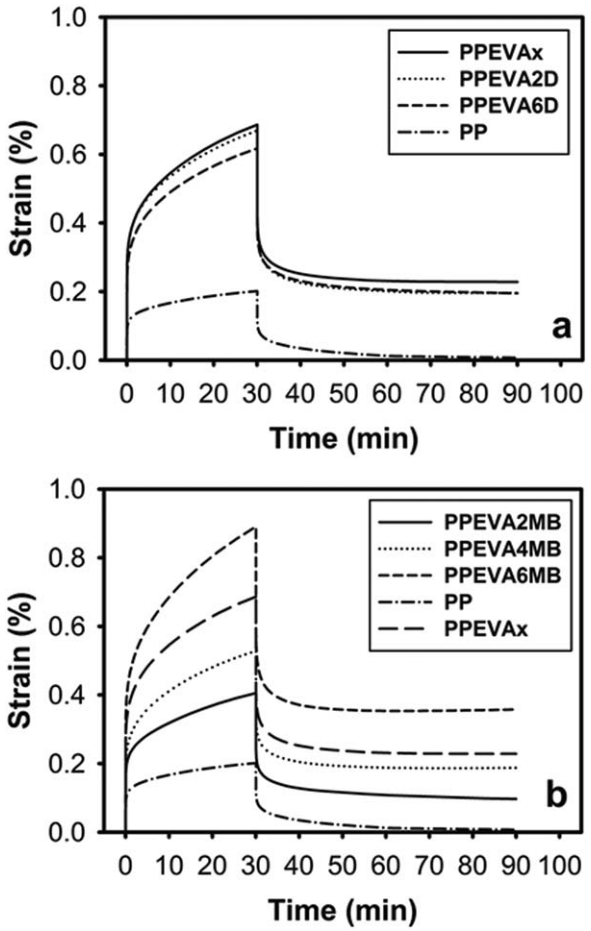

Figure 13. Creep-recovery strain versus time of: a) PP homopolymer, PPEVAx and PP-EVA/clay nanocomposites obtained by direct strategy and b) PP homopolymer, PPEVAx and PP-EVA/clay nanocomposites obtained by masterbatch strategy.

Table V. Creep and Recovery Strain Parameters for PP Homopolymer, PPEVAx Sample, and the PP-EVA/Clay Nanocomposites Samples Obtained by Direct (D) and Masterbatch (MB) Strategies

Sample	ε_e^{cr} (%)	ε_{max}^{cr} (%)	ε_e^{rec} (%)	ε_{vp} (%)
PP	0.07	0.20	0.10	0.01
PPVAx	0.25	0.69	0.36	0.23
PPEVA2D	0.25	0.67	0.33	0.20
PPEVA6D	0.21	0.62	0.33	0.20
PPEVA2MB	0.15	0.34	0.23	0.10
PPEVA4MB	0.17	0.54	0.32	0.19
PPEVA6MB	0.29	0.89	0.54	0.36

Figure 12 shows the Tan δ results for both types of PP-EVA/clay nanocomposites. Figure 12(a) corroborates the immiscibility of PPEVAx sample, however some compatibility between phases was also observed due to the dynamic crosslinking reaction, especially in the PPEVA6D sample. In addition, it is observed that the peak corresponding to the EVA Tg (around −19.4°C) decrease with the introduction of the modified nanoclay (−21.4°C) and the Tan δ peak intensity of this sample decreased due to the increase of chain mobility at low nanoclay concentration and the reduction of this property at higher nanoparticles concentration.[27] On the other hand, the Tan δ results of PP-EVA/clay nanocomposites prepared through masterbatch strategy [Figure 12(b)] show that as the EVA content increases, the peak corresponding to the EVA Tg (around −20.2°C) increased their intensity. Additionally, the T_g of PPEVA6MB sample increased (18.9°C), indicating a reduction in the chain mobility of this sample due to the high degree of crosslinking and high nanoclay concentration.

The analysis of the creep-recovery behavior of PP-EVA/clay nanocomposites obtained using direct and masterbatch clay introduction strategies was performed with the strain (%) versus time (min) traces. Figure 13(a) displays the creep and recovered strain as a function of time for PPEVAx and PP-EVA/clay nanocomposites obtained from the direct strategy. In the experimental tests, 1 MPa was selected as the applied stress within the elastic range. These curves present typical viscoelastic–viscoplastic behavior (instantaneous deformation, primary and secondary creeps). As expected, the creep strain reduced with increased clay concentration.[49] This improvement in creep can be attributed to a restriction in the slippage, reorientation and motion of the PP-EVA polymer chains due to the presence of the nanoparticles.[50–53] For example, the elastic creep strain (ε_e^{cr}) and maximum creep strain (ε_{max}^{cr}) were reduced from 0.25% and 0.69% for the PPEVAx sample to 0.21% and 0.62% for the PPEVA6D sample, respectively.

The sequence of the recovered strain as a function of time is also presented in Figure 10(a). These curves indicate that the incorporation of nanoclays improved the elastic recovery; however, the nanoclays slightly decreased the recovered strain. It was found that the elastic recoverable strain (ε_e^{rec}) and the viscoplastic recoverable strain (ε_{vp}) of the nanocomposites were not highly influenced by the clay concentration (e.g., 0.36% and 0.23% for the PPEVAx sample and 0.33% and 0.20% for both PP-EVA/clay nanocomposites, respectively). This behavior can be due to the high flexibility of the PP-EVA macromolecular chains; even at high concentrations of nanoparticles,[54–56] or due to the decrease in the polymer-filler interactions, such as it was recently reported in a stress relaxation analysis of natural rubber/nitrile rubber/clay nanocomposites.[31] Creep recovery is particularly significant in engineering applications. For example, if the unrecovered strain is large after removing the applied stress, the material would suffer unpredictable damage. In this sense, the results of creep recovery obtained for PP-EVA/clay nanocomposites prepared through the direct clay introduction strategy indicate that these materials have low possibilities to suffer unpredictable damage during their possible engineering applications.

Figure 13(b) shows the creep-recovery strain as a function of time for PP-EVA/clay nanocomposites obtained via the masterbatch strategy. The experiment was also performed at an applied stress of 1 MPa, and all curves presented a viscoelastic-viscoplastic behavior. However, it is observed that the creep strain for these nanocomposites presents an inverse relation to clay concentration. For example, the elastic creep strain (ε_e^{cr}) and maximum creep strain (ε_{max}) for the PPEVA2MB sample were 0.15% and 0.34%, respectively, while for the PPEVA4MB sample, they were 0.17% and 0.54%, and for the PPEVA6MB sample, they were 0.29% and 0.84%. Nevertheless, this behavior can be explained in terms of the different EVA concentrations in each PP-EVA/clay nanocomposite. EVA chains have greater mobility than PP chains; therefore, higher concentrations of EVA enhanced the elasticity of the PP-EVA/clay nanocomposites obtained using the masterbatch strategy. This chain mobility was not greatly affected by the nanoclay presence, the possible PP-EVA grafting or EVA crosslinking.

The sequence of the recovered strain as a function of time is also presented in Figure 13(b). These curves indicate that incorporation of nanoclays improved the elastic recovery but slightly decreased the recovered strain. It was found that the elastic recoverable strain (ε_e^{rec}) and the viscoplastic recoverable strain (ε_{vp}) of the nanocomposites were highly influenced by the EVA concentration (i.e., 0.23% and 0.10% for the PPEVA2MB sample, 0.19% and 0.32% for PPEVA4MB, and 0.54% and 0.36% for PPEVA6MB). Finally, the creep-recovery behavior for PP-EVA/clay nanocomposites obtained using the masterbatch strategy indicated that the PPEVA2MB sample had better mechanical stability under constant load and on removal of the load. The behavior of this nanocomposite was close to the polypropylene homopolymer behavior (see Table V).

CONCLUSIONS

The reaction of PP and EVA chains, using DCP as the initiator, mainly generated a PP-EVA chemical bond, which helped to enhance the compatibility between the PP and EVA phases, and the interaction between nanoclay sheets and PP-EVA chains producing nanocomposites with intercalated nanoclay sheets, mainly located in the co-continuous EVA-PP interfaces, for the direct strategy, and PP-EVA/clay nanocomposites with exfoliated

nanoclay sheets mainly located in the EVA domains of a droplet (2 wt % clay) or co-continuous (6 wt % clay) blend morphology, due to the high covalent interactions between EVA and nanoclays sheets, for the masterbatch strategy.

The clay introduction strategy had also a significant effect on the dynamic mechanical properties at low temperatures, the melt flow and the creep-recovery behavior of PP-EVA/clay nanocomposites in terms of the chain mobility and chain relaxation, generating PP-EVA/clay nanocomposites with a wide range of mechanical (e.g. stiffness, creep resistant, and creep recovery) and rheological properties. These properties can be exploited by different engineering applications, such as automotive industry, which usually required materials with high stiffness where appearance, moldability, dimensional conformity, or low weight can be promoted by the use of these materials.

ACKNOWLEDGMENTS

This work was financially supported by the National Research Council of Science and Technology of Mexico (CONACYT) through grants U40177-Y and 57070. The authors also thank J. G. Rodríguez-Velasquez, E. Díaz-Barriga, M de L. Guillén-Cisneros, M. G. Méndez-Padilla, V. Comparán-Padilla, Myriam Lozano, and A. Torres-Martínez for their important contribution to the experimental measurements and suggestions, which helped in the development of this work.

REFERENCES

1. Alexandre, M.; Dubois, Ph. *Mater. Sci. Eng.* **2000**, *28*, 1.
2. Ray, S. S.; Okamoto, M. *Prog. Polym. Sci.* **2003**, *28*, 1539.
3. Pavlidoua, S. Papaspyrides, C.D. *Prog. Polym. Sci.* **2008**, *33*, 1119.
4. Cho, J. W.; Paul, D. R. *Polymer* **2001**, *42*, 1083.
5. Gawad, A. A.; Esawi, A. M. K.; Ramadan, A. R. *J. Mater. Sci.* **2010**, *45*, 6677.
6. Barbas, J. M.; Machado, A. V.; Covas, J. A. *Chem. Eng. Technol.* **2014**, *37*, 257.
7. Pasanovic-Zujo, V.; Gupta R. K.; Bhattacharya S. N. *Rheol. Acta* **2004**, *43*, 99.
8. Gelfer, M. Y.; Burger Ch.; Chu B.; Hsiao B. S.; Drozdov A. D.; Si M.; Rafailovich M.; Sauer B. B.; Gilman J. W.; *Macromolecules* **2005**, *38*, 3765.
9. Fornes, T. D.; Yoon, P. J.; Hunter, D. L.; Keskkula, H.; Paul, D. R. *Polymer* **2002**, *43*, 5915.
10. Yoon, P. J.; Hunter, D. L.; Paul, D. R. *Polymer* **2003**, *44*, 5323.
11. Thomas, S.; George, A. *Eur. Polym. J.* **1992**, *28*, 1451.
12. Ramírez-Vargas, E.; Navarro-Rodríguez, D.; Medellín-Rodríguez, F. J.; Huerta-Martínez, B. M.; Lin, J. S. *Polym. Eng. Sci.* **2000**, *40*, 2241.
13. Bhattacharya, S.; Gupta, R. K.; Bhattacharya, S. N. *Polym. Eng. Sci.* **2010**, *50*, 1350.
14. Goodarzi, V.; Jafari S. H.; Khonakdar, H. A.; Seyfi, J. *J. Polym. Res.* **2011**, *18*, 1829.
15. Goodarzi, V.; Jafari, S. H.; Khonakdar, H. A.; Hässler, R.; Reuter, U. *J. Appl. Polym. Sci.* **2012**, *125*, 922.
16. Martins, C. G.; Larocca, N. M.; Paul, D.R.; Pessan, L.A. *Polymer* **2009**, *50*, 1743.
17. Ray, S. S.; Pouliot, S.; Bousmina, M.; Utracki, L. A. *Polymer* **2004**, *45*, 8403.
18. Tiwari, R. R.; Paul, D. R. *Polymer* **2011**, *52*, 1141.
19. Lee, H. -S.; Fasulo, P. D.; Rodgers, W. R.; Paul, D. R. *Polymer* **2005**, *46*, 11673.
20. Si, M.; Araki, T.; Ade, H.; Kilcoyne, A. L. D.; Fisher, R.; Sokolov, J. C.; Rafailovich, M. H. *Macromolecules* **2006**, *39*, 4793.
21. Ramírez-Vargas, E.; Medellín-Rodríguez, F. J.; Navarro-Rodríguez, D.; Ávila-Orta, C. A.; Solís-Rosales, S. G.; Lin, J. S. *Polym. Eng. Sci.* **2002**, *42*, 1350.
22. Huerta-Martínez, B. M.; Ramírez-Vargas, E.; Medellín-Rodríguez, F. J.; Cedillo, G. R. *Eur. Polym. J.* **2005**, *41*, 519.
23. Valera-Zaragoza, M.; Ramírez-Vargas, E.; Medellín-Rodríguez, F. J.; Huerta-Martínez, B. M.; *Polym. Degrad. Stab.* **2006**, *91*, 1319.
24. Valera-Zaragoza, M.; Ramírez-Vargas E.; Medellín-Rodríguez, F. J. *J. Appl. Polym. Sci.* **2008**, *108*, 1986.
25. Ramírez-Vargas E., Valera-Zaragoza M., Sánchez-Valdés S., Hernández-Valdez JS., Ibarra-Castillo, F. F. *Polym. Bull.* **2009**, *62*, 391.
26. Espinoza-Martínez, A. B.; Ramírez-Vargas, E.; Sánchez-Valdés, S.; Ramos de Valle, L. F.; Medellín-Rodríguez, F. J.; Hsiao, B. S.; Rong, L.; Valera-Zaragoza, M. *J. Appl. Polym. Sci.* **2013**, *128*, 3473.
27. Valera-Zaragoza, M.; Rivas-Vázquez, L. P.; Ramírez-Vargas, E.; Sánchez-Valdés, S.; Ramos-de Valle, L. F.; Medellín-Rodríguez, F. J. *Compos B* **2013**, *55*, 506.
28. Katbab, A. A.; Nazockdast, S.; Bazgir, S. *J. Appl. Polym. Sci.* **2000**, *75*, 1127.
29. Wang, K.; Liang, S.; Deng, J.; Yang, H.; Zhang, Q.; Fu, Q.; Dong, X.; Wang, D.; Han, Ch. C. *Polymer* **2006**, *47*, 7131.
30. Pistor,V.; Ornaghi, H. L.; Ferreira, C. A.; Zattera, A. J. *J. Appl. Polym. Sci.* **2012**, *125*, E462.
31. Maria, H. J.; Lyczko, N.; Nzihou, A.; Joseph, K.; Mathew, Ch.; Thomas, S. *Appl. Clay Sci.* **2014**, *87*, 120.
32. Babu R. R.; Naskar, K. *Adv Polym Sci.* **2011**, *239*, 219.
33. Passador, F. R.; Alzate-Rojas, G. J.; Pessan, L. A. *J. Macromol. Sci. Part B: Phys.* **2013**, *52*, 1127.
34. Joubert, C.; Cassagnau, Ph.; Michel, A. *Polym. Eng. Sci.* **2002**, *42*, 2222.
35. John, B.; Varughese, K. T.; Oommen, Z.; Thomas, S. *Polym. Eng. Sci.* **2010**, *50*, 665.
36. Okamoto, M.; Nam, P. H.; Maiti, P.; Kotaka, T.; Hasegawa, N.; Usuki, A.; *Nano Lett.* **2001**, *1*, 295.
37. Zhang, R.; Zhu, Y.; Zhang, J.; Jiang, W.; Yin, J. *J. Polym. Sci. Part A: Polym. Chem.* **2005**, *43*, 5529.
38. Maciel, A.; Salas, V.; Manero, O. *Adv. Polym. Technol.* **2005**, *24*, 241.
39. Cao, K.; Shen, Z-Ch.; Yao, Z.; Qub, B.-W.; Pang, X.-B.; Lu, Z.-Q.; Li, Y.; Chen, Z.-H. *Chem. Eng. Sci.* **2010**, *65*, 1621.
40. Dalai, S.; Wenxiu, Ch. *J. Appl. Polym. Sci.* **2002**, *86*, 3420.

41. Dikobe, D. G.; Luyt, A. S. *eXPRESS Polym. Lett.* **2009**, *3*, 190.
42. Liu, L.; Wang, Y.; Li, Y.; Wu, J.; Zhou, Z.; Jiang, Ch. *Polymer* **2009**, *50*, 3072.
43. Kakkar, D.; Maiti, S. N. *J. Appl. Polym. Sci.* **2012**, *123*, 1905.
44. Vaia, R. A.; Gianellis, E. P. *Macromolecules* **1997**, *30*, 8000.
45. Morgan, A. B.; Gilman, J. W. *J. Appl. Polym. Sci.* **2003**, *87*, 1329.
46. Koo, Ch. M.; Kim, M. J.; Choi, M. H.; Kim, S. O.; Sang O.; Chung, I. J. *J. Appl. Polym. Sci.* **2003**, *88*, 1526.
47. Rao, Y. Q.; Pochan, J. M. *Macromolecules* **2007**, *40*, 290.
48. Sharma, S. K.; Nayak, S. K. *Polym. Degrad. Stab.* **2009**, *94*, 132.
49. Menard, K. P. Dynamic Mechanical Analysis: A Practical Introduction, 2nd ed.; CRC Press: Boca Raton (**2008**).
50. Zhang, Z.; Yang, J. -L.; Friedrich, K.; *Polymer* **2004**, *45*, 3481.
51. Yang, J.; Zhang, Z.; Friedrich, K.; Schlarb, A. K. *Macromol. Rapid Commun.* **2007**, *28*, 955.
52. Drozdov, A. D.; Lejre, A. -L. -H.; Christiansen, J. deC. *Compos. Sci. Technol.* **2009**, *69*, 2596.
53. Shokuhfar, A.; Zare-Shahabadi, A.; Atai, A. -A.; Ebrahimi-Nejada, S.; Termeha, M. *Polym. Test.* **2012**, *31*, 345.
54. Siengchin, S.; Karger-Kocsis, J. *Macromol. Rapid Commun.* **2006**, *27*, 2090.
55. Jia, Y.; Peng, K.; Gong, X-L.; Zhang, Z. *Int. J. Plast.* **2011**, *27*, 1239.
56. Starkova, O.; Buschhorn, S.T.; Mannov, E.; Schulte, K.; Aniskevich, A. *Compos. A* **2012**, *43*, 1212.